J. Fluid Mech. (1994), *vol.* 280, *pp.* 149–172

Shear dispersion and anomalous diffusion by chaotic advection†

By S. W. JONES‡ AND W. R. YOUNG

Scripps Institution of Oceanography, University of California at San Diego, La Jolla, CA 92093, USA

(Received 28 November 1989 and in revised form 8 June 1994)

The dispersion of passive scalars by the steady viscous flow through a twisted pipe is both a simple example of chaotic advection and an elaboration of Taylor's classic shear dispersion problem. In this article we study the statistics of the axial dispersion of both diffusive and perfect (non-diffusive) tracer in this system.

For *diffusive* tracer chaotic advection assists molecular diffusion in transverse mixing and so diminishes the axial dispersion below that of integrable advection. As in many other studies of shear dispersion the axial distribution ultimately becomes Gaussian as $t \to \infty$. Thus there is a diffusive regime, but with an effective diffusivity that is enhanced above molecular values. In contrast to the classic case, the effective diffusivity is not necessarily inversely proportional to the molecular diffusivity. For instance, in the irregular regime the effective diffusivity is proportional to the *logarithm* of the molecular diffusivity.

For *perfect* tracer chaotic advection does not result in a diffusive process, even in the irregular regime in which streamlines wander throughout the cross-section of the pipe. Instead the variance of the axial position is proportional to $t \ln t$ so that the measured diffusion coefficent diverges like $\ln t$. This faster than linear growth of variance is attributed to the trapping of tracer for long times near the solid boundary, where the no-slip condition ensures that the fluid moves slowly. Analogous logarithmic effects associated with the no-slip condition are well known in the context of porous media.

A simple argument, based on Lagrangian statistics and a local analysis of the trajectories near the pipe wall, is used to calculate the constants of proportionality before the logarithmic terms in both the large- and infinite-Péclet-number limits.

1. Introduction and background

When a very viscous fluid is pumped slowly through a straight pipe the velocity distribution is the well-known Poiseuille profile with a maximum at the centre of the duct and no motion at the wall. Taylor (1953) realized that because of this transverse shear a dissolved, passive solute is differentially advected so that initial gradients in concentration are amplified. The separation of two molecules initially on different streamlines increases linearly with time and consequently the mean-square displacement, $\sigma^2(t)$, of the ensemble of molecules about the centre of mass, $\bar{z}$, increases quadratically with time (z is the longitudinal or axial coordinate and $\sigma^2(t)$ and $\bar{z}$ are formally defined in (1.9) below).

† With an Appendix by J. F. Brady

‡ Present address: Department of Theoretical and Applied Mechanics, University of Illinois, Urbana, IL 61801-2935, USA

Central to Taylor's theory is the realization that both gradient amplification and quadratic growth of $\sigma^2(t)$ are ultimately arrested by the molecular diffusion of the tracer. This balance is achieved on times long compared to the diffusion time of a solute molecule across the transverse section of the pipe. Molecular diffusivity prevents the solute gradients from growing without bound and also makes the separation of molecules less efficient. In fact the mean square-displacement ultimately grows only linearly with time

$$\sigma^2(t) \sim 2D_* t \qquad \text{as} \qquad t \to \infty, \tag{1.1}$$

where D_* is the effective axial diffusivity. For a circular pipe with cross-sectional area $A = \pi a^2$ the effective diffusivity is

$$D_* = D_{\text{mol}} + \frac{W^2 A}{48\pi D_{\text{mol}}}, \tag{1.2}$$

where W is the sectionally averaged axial velocity and D_{mol} is the molecular diffusivity. When the molecular diffusivity of the solute is small the last term in (1.2) is much larger than the second and the effective diffusivity is inversely proportional to the molecular diffusivity.

This basic dispersion problem has been elaborated in many different ways. In this article we are concerned with the effects of a secondary flow in the transverse direction. Secondary circulation is generated by curving the pipe (Dean 1927, 1928) and its effect on shear dispersion was assessed by Erdogan & Chatwin (1967), Nunge, Lin, & Gill (1972) and more recently by Johnson & Kamm (1986). The principal conclusion of these authors is that because the secondary flow produces transverse mixing it aids molecular diffusivity in preventing the growth of contaminant gradients. This enhanced transverse mixing reduces the effective axial diffusivity relative to that in a straight pipe.

In these earlier works the trajectory of a *perfect* tracer particle (i.e. a particle that does not diffuse) is integrable. This is because the geometry of the pipe is simple and the streamlines are confined to streamsurfaces, or equivalently, KAM tori. Molecular diffusion is essential in enabling a solute molecule to escape from these two-dimensional surfaces and completely sample the transverse cross-section of the pipe. In fact, as in Taylor's original investigation, $\sigma^2(t)$ for an ensemble of perfect tracer particles grows quadratically with time, while for diffusive tracer particles it eventually increases only linearly with time. And, as in (1.2), the effective diffusivity is inversely proportional to the molecular diffusivity. Jones, Thomas, & Aref (1989, JTA hereafter) consider the possibility that the trajectory of a perfect tracer particle is chaotic in the steady, three-dimensional velocity field within the pipe. This is an example of 'chaotic advection' (Aref 1984). JTA study steady viscous flow in an infinite 'twisted pipe' consisting of a sequence of semi-circular pipe segments as shown in figure 1. The twist arises because the plane of each semi-circular segment is at a fixed angle, χ, to the preceding one. If χ equals either 0 or π then the pipe lies in a plane and the resulting dynamical system for the particle trajectories is integrable, i.e. all of the streamlines are confined to two-dimensional streamsurfaces. We refer to this completely integrable flow as the *regular* regime. This is the case considered by Johnson & Kamm (1986) and virtually all preceding authors.

However if χ is not equal to either 0 or π then the pipe does not lie in a plane and the trajectories of particles advected by this steady flow can be non-integrable so that some streamlines are not confined to streamsurfaces and instead they wander through a three-dimensional subregion within the pipe. When the perturbation of the

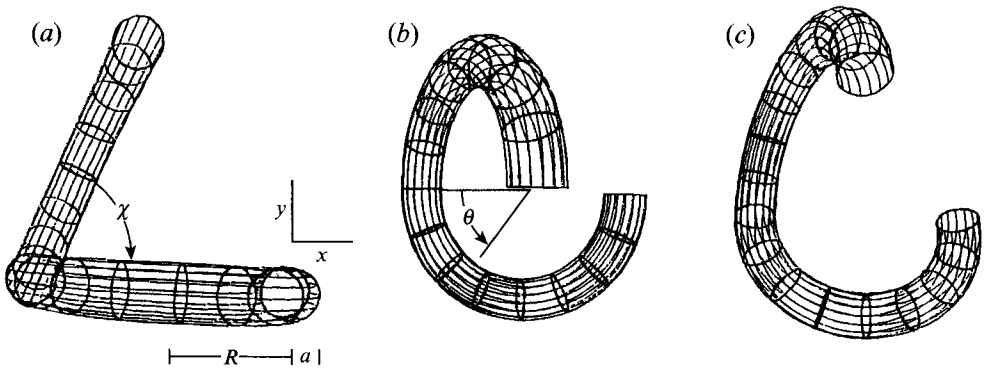

FIGURE 1. Perspective drawings of the periodic 'basic cell' used in this study. The cell is composed of two 180° curved pipe segments with constant radius of curvature. The coordinate system used to describe the flow is also shown (from JTA 1989, figure 1).

integrable system is weak (e.g. χ is close to 0 or π) some streamlines remain confined to two-dimensional streamsurfaces, while others tangle in a three-dimensional region. As in dynamical systems theory (e.g. Lichtenberg & Lieberman 1982) the former streamlines define regions of regular motion ('islands') while the latter define regions of irregular motion (the chaotic 'sea'). This complicated structure, in which domains of regular and irregular flow coexist, will be referred to as the *mixed* regime. These features are generic to near-integrable dynamical systems and have been documented by JTA for the twisted pipe.

As the strength of the perturbation increases, the volume occupied by regular regions decreases as streamsurfaces break up. In fact we show in §3 that when χ equals $\pi/2$, and the secondary flow is sufficiently strong, the streamlines wander throughout the cross-section of the pipe. There may still be some small islands of integrability but these occupy a negligible fraction of the volume and they are no longer absolute barriers to the transport of perfect tracer particles in the transverse section of the pipe. We refer to this as the *irregular* regime.

At this point we should note the study of Saxena & Nigam (1984), who measured the residence time distribution for a passive scalar advected through a series of helical coils that, like the twisted pipe, are joined with a non-zero angle between the axes of coiling. The results of their experiments indicate that periodically changing the orientation of the helical coil diminishes the effective diffusivity.

Our goal is to understand the dispersion of both perfect and diffusive tracer particles in these three different regimes. Table 1 summarizes both our conclusions and those of earlier authors. The regular case is Taylor's classic shear dispersion problem and is well understood. The breakup of the streamsurfaces in the mixed case is discussed in detail by JTA. That work focuses on particle dispersion in the *transverse* plane of the pipe. Section 3 of the present paper emphasizes the *axial* dispersion of tracer in this mixed regime. The mixed regime is the most complicated of the three cases and our results are mostly direct numerical integration and scale analysis. Numerical experiments in the irregular regime are presented in §3. In this case there are no streamsurfaces to restrict transverse motion and it is possible to analytically calculate effective diffusivities and compare these with simulation. This is done in §4. Thus the irregular regime is easier to analyse than the mixed regime.

Flow geometry	Perfect tracer	Diffusive tracer
Straight pipes (regular regime)	Taylor (1953) $\sigma^2(t) \sim W^2t^2$	Taylor (1953) $\sigma^2(t) \sim D_{\mathrm{mol}}Pe^2t$
Curved pipes (regular regime)	No explicit references $\sigma^2(t) \sim W^2t^2$	Erdogan & Chatwin (1967) Nunge, *et al.* (1972) Johnson & Kamm (1986) $\sigma^2(t) \sim D_{\mathrm{mol}}Pe^2t$
Twisted pipes (mixed regime)	Jones *et al.* (1989) $\sigma^2(t) \sim W^2t^2$	This paper $\sigma^2(t) \sim D_{\mathrm{mol}}Pe^2t$
Twisted pipes (irregular regime)	This paper $\sigma^2(t) \sim D_{\mathrm{mol}}Pe\,t\ln t$	This paper $\sigma^2(t) \sim D_{\mathrm{mol}}Pe\ln Pe\,t$

TABLE 1. Selected papers on shear dispersion in pipes and the asymptotic ($t \to \infty$) scaling for the axial variance

One might guess that this simplicity in the irregular regime arises because all of the essential ingredients of Taylor's original theory are present even for perfect tracer. There is an axial flow with a maximum in the middle of the channel and no motion at the walls. Complete transverse mixing is provided by the non-integrable secondary flow. This chaotic transverse mixing ensures that the velocity of the centre of mass of an ensemble of perfect tracer molecules is equal to the sectionally averaged axial velocity, W. (This is not the case in the regular and mixed regimes where the ensemble-averaged velocity depends on the initial locations of the particles.) This same transverse mixing should act to prevent the growth of tracer gradients created by shear in the axial component of velocity. One is tempted to speculate that in the irregular regime $\sigma^2(t)$ for an ensemble of perfect tracer particles should grow linearly with time. Further, a tracer with a very small molecular diffusivity might behave effectively like a perfect tracer and disperse with an effective axial diffusivity that is independent of its small molecular diffusivity. This is in sharp contrast to the regular regime in which the effective diffusivity is inversely proportional to the molecular diffusivity.

These intuitively plausible expectations are frustrated by the results reported below. We find that $\sigma^2(t)$ for an ensemble of perfect tracer particles in the irregular regime grows slightly faster than linearly with time, as $t\ln t$, and the concentration profiles are persistently skew. This is the case even when there is complete transverse mixing by the non-integrable velocity field. Further, the effective diffusivity of a solute with a very small molecular diffusivity is inversely proportional to the logarithm of the molecular diffusivity.

One must conclude that the analogy between transverse mixing due to chaotic advection and molecular diffusion is faulty. Perhaps this is not entirely surprising but there is a second line of argument that also incorrectly concludes that $\sigma^2(t)$ for an ensemble of perfect tracer particles in the irregular regime should grow linearly with time. This reasoning was advanced by Taylor (1954) in the context of shear dispersion in a fully turbulent pipe flow. It was again employed by Erdogan & Chatwin (1967) to conclude, before any detailed calculation, that there is an effective axial diffusivity governing the dispersion of tracer in a curved pipe.

This reasoning is based on Taylor's (1921) expression for the rate of change of $\sigma^2(t)$

and the effective diffusivity D_*:

$$\frac{\mathrm{d}\sigma^2(t)}{\mathrm{d}t} = 2\int_0^t \mathscr{C}(t_1)\,\mathrm{d}t_1 \to 2D_* \quad \text{as} \quad t \to \infty, \tag{1.3}$$

where $\mathscr{C}(t)$ is the autocorrelation function of the axial velocity of a particle relative to the velocity of the centre of mass of the ensemble, W. Denoting this relative axial velocity by $w'(t) = w(t) - W$, we have

$$\mathscr{C}(t) \equiv \overline{w'(0)w'(t)}, \tag{1.4}$$

where the overbar is the ensemble average used below in (1.9).

The expression (1.3) requires that there is no variation in the statistical properties of the flow in the axial direction. The twisted pipe flow satisfies this assumption, at least on moderately long times when the ensemble is spread over many semi-circular segments. However the difficulty is that for perfect tracer particles the integral in (1.3) does not approach a constant as $t \to \infty$. In fact we find below that in the irregular regime at large times

$$\mathscr{C}(t) \sim \frac{p}{t}. \tag{1.5}$$

From (1.5) it follows that $\sigma^2(t) \sim 2pt\ln t$ at large times.

For diffusive tracer the correlation decays slowly as in (1.5) only when

$$t < Pe^{1/3}a^2/\Psi. \tag{1.6}$$

Here $Pe \sim \Psi/D_{\mathrm{mol}}$, where Ψ is the magnitude of the streamfunction for the secondary flow in the transverse plane and Pe is the Péclet number of this secondary circulation (a more precise definition of Pe is given below in (2.12)). At longer times molecular diffusion becomes important and produces an exponentially decaying correlation

$$\mathscr{C}(t) \sim \mathrm{e}^{-\mu t} \quad \text{when} \quad t > a^2Pe^{1/3}/\Psi, \quad \text{where} \quad \mu^{-1} \sim a^2Pe^{1/3}/\Psi. \tag{1.7}$$

The scaling $Pe^{1/3}$ in (1.6) and (1.7) is obtained with standard arguments based on a local analysis of the advection–diffusion equation near a no-slip boundary. And fortunately it is not necessary to calculate μ in order to find the leading-order approximation to the effective diffusivity, D_*. Substituting (1.5) into (1.3) and stopping the integration when $t \sim Pe^{1/3}a^2/\Psi$ gives the leading-order result

$$D_* \approx \frac{p}{3}\ln Pe. \tag{1.8}$$

Below we calculate p with a simple statistical argument and successfully compare (1.8) with simulations of particle dispersion in the irregular regime.

The slow decay of the correlation function in (1.5) is an example of long-time correlations in a dynamical system. These persistent correlations can arise because irregular trajectories are trapped near regions of regular motion (islands of integrability) for long periods (Karney 1983; Meiss & Ott 1986). Here we propose a different trapping mechanism for the algebraic tail: because of the no-slip condition particles remain near the wall of the pipe for long sojourns.

The 'no-slip' trapping mechanism is the same as in de Josselin de Jong's (1958) and Saffman's (1959) models of dispersion in a porous medium and the 'logarithmic' effects we have mentioned above are well known in this context. (The volume edited by Guyon, Nadal & Pomeau 1988 is a good survey of both theoretical and experimental studies of dispersion in porous media.) Indeed the results in (1.5)–(1.8) are analogous to those reported by Koch & Brady (1985, 1987), Baudet, Guyon, & Pomeau (1985),

and Young & Jones (1991) in which an unconsolidated porous medium is modelled as a dilute ensemble of identical solid spheres (radius a) fixed at random points in space. Viscous fluid flows with a bulk velocity W around the spheres. Because of the no-slip condition tracer is trapped at the surface of the spheres for long intervals, and for perfect tracer this results in a correlation function with an algebraic tail as in (1.5) with $p \sim \phi a W$, where ϕ is the volume fraction of solid. The correlation function of diffusive tracer has a similar structure provided an inequality analogous to (1.6) is satisfied. At longer times the molecular diffusivity becomes important and produces the asymptotic results in (1.7) and (1.8) with $Pe \equiv aW/D_{\mathrm{mol}}$.

For reference we now note the standard definition of the centre of mass, and the mean-square displacement about this position, of an ensemble of particles. If N is the total number of particles in the ensemble and z_i is the axial position of the ith particle then

$$\sigma^2(t) \equiv \overline{(z-\bar{z})^2} = \frac{1}{N}\sum_{i=1}^{N}(z_i-\bar{z})^2, \quad \text{where} \quad \bar{z} \equiv \frac{1}{N}\sum_{i=1}^{N} z_i. \tag{1.9}$$

2. The model flow

We have studied the incompressible flow of a viscous fluid through a twisted pipe of circular cross-section. This flow yields chaotic particle trajectories. A complete description of the equations of motion and documentation of the chaotic behavior are presented by JTA. In this section we briefly review the essential features of relevance to this paper.

The basic flow element is a section of curved pipe. This section is bent, with constant radius of curvature R, through π radians and is joined to a similar section with a pitch angle χ between them. This two-section 'basic cell', shown in figure 1, is repeated periodically. χ is the sole parameter governing the pipe geometry. For $\chi = 0$ the twisted pipe degenerates to a torus. For $\chi = \pi$ the pipe again lies in a plane and the basic cell is S-shaped.

The equations of motion for flow through a curved pipe have been derived by Dean (1927, 1928) by means of a regular perturbation expansion in powers of the Dean number, $De \equiv Re^2(a/R)$, where Re is the Reynolds number, $Re \equiv Wa/\nu$, and ν is the kinematic viscosity. The fundamental perturbation assumption is that the radius of the cross-section is much smaller than the radius of curvature ($a \ll R$). Using primes to denote dimensional variables, the lowest-order solution for the transverse streamfunction and axial velocity is

$$\psi' = \frac{\nu De}{72}\left(4-\frac{r'^2}{a^2}\right)\left(1-\frac{r'^2}{a^2}\right)^2\frac{y'}{a} \quad \text{and} \quad \dot{z}' = 2W\left(1-\frac{r'^2}{a^2}\right), \tag{2.1}$$

where $r'^2 \equiv x'^2 + y'^2$. Thus the scale of the transverse streamfunction used above in (1.6) and (1.7) is $\Psi \equiv \nu De/72$. To obtain the non-dimensional advection equations we introduce

$$(x', y') = a(x, y), \quad t' = \frac{R}{W}t, \quad \psi' = \frac{Wa^2}{R}\psi, \tag{2.2}$$

and to emphasize the correspondence between the axial coordinate and an angle we use the notation

$$z' = R\theta, \tag{2.3}$$

so that the unit cell is $0 < \theta < 2\pi$. In terms of these non-dimensional variables the

trajectory of a molecule of perfect tracer is obtained from

$$\dot{x} = -\psi_y, \qquad \dot{y} = \psi_x, \qquad \dot{\theta} = 2(1 - r^2), \tag{2.4}$$

where the non-dimensional streamfunction is

$$\psi = \frac{Re}{72}(4 - r^2)(1 - r^2)^2 y, \tag{2.5}$$

and $r^2 \equiv x^2 + y^2$.

The model for perfect particles flowing through a twisted pipe consists of a sequence of Dean solutions and an appropriate rotation at the end of each segment. Thus the advection of a particle through one basic cell has the symbolic representation $A = TMTM$ where M is the mapping of a particle from the cross-section at $\theta = 0$ to the cross-section at $\theta = \pi$ and T is a rotation of the particle by an angle $-\chi$. For sufficiently large Re the flow is chaotic if $0 < \chi < \pi$. The two limits $\chi = 0$ and π lead to integrable particle trajectories for all values of Re. For fixed Re the size of the regular islands diminishes as χ approaches $\pi/2$.

Note that in this model the flow possesses a velocity discontinuity at the intersection of curved pipe sections. The effects of this artifact of the model are more completely discussed in JTA. Here we remark that the feature responsible for the chaotic particle motion is the breaking of the toroidal symmetry of the pipe geometry. It is the twist, not the discontinuity, which introduces θ dependence into the advection equations and makes them non-integrable.

To model the motion of diffusive particles the deterministic flow solution described above is augmented by a series of stochastic displacements. Thus the dimensional equations of motion become the generalized Langevin equations

$$\dot{x}' = u'(x', t') + \zeta'(t'), \tag{2.6}$$

where the velocity vector, u', is given by the dimensional form of (2.5) and the stochastic term ζ' is a set of Gaussian random deviates with autocorrelation

$$\overline{\zeta_i'(t_1')\zeta_j'(t_2')} = 2D_{\text{mol}}\,\delta_{ij}\,\delta(t_1' - t_2'). \tag{2.7}$$

We have confined our attention to tracer that diffuses only in the pipe cross-section.

A non-dimensional molecular diffusivity, D, is obtained from the dimensional molecular diffusivity, D_{mol}, by consideration of the tracer conservation equation in dimensional variables

$$C_{t'} + J(\psi', C) + 2W\left(1 - \frac{r'^2}{a'^2}\right) C_{z'} = D_{\text{mol}}(\partial_{x'}^2 + \partial_{y'}^2)\, C, \tag{2.8}$$

where the Jacobian, $J(a, b)$, is

$$J(a, b) \equiv \frac{\partial a}{\partial x'}\frac{\partial b}{\partial y'} - \frac{\partial b}{\partial x'}\frac{\partial a}{\partial y'}. \tag{2.9}$$

Using the scalings in (2.2)–(2.4) the non-dimensional advection–diffusion equation is

$$C_t + J(\psi, C) + 2(1 - r^2)\, C_\theta = D(\partial_x^2 + \partial_y^2)\, C, \tag{2.10}$$

where $\psi(x, y)$ is defined in (2.5) and the non-dimensional diffusivity is

$$D = \frac{RD_{\text{mol}}}{Wa^2}. \tag{2.11}$$

In §1 we introduced the Péclet number of the transverse flow. We can now give a

more precise definition of this crucial non-dimensional parameter. It is the ratio of the coefficent of ψ in the second term in (2.10) to the coefficent of the last term. That is

$$Pe \equiv \frac{Re}{72D} = \frac{1}{72}\frac{a}{R}\frac{W^2a^2}{\nu D_{\mathrm{mol}}} = \frac{De}{72}\frac{\nu}{D_{\mathrm{mol}}}. \tag{2.12}$$

3. Simulation of shear dispersion in a twisted pipe

In this section we present numerical simulations of both diffusive and perfect tracer dispersion in the twisted pipe.

3.1. *Axial dispersion*

In JTA the coupling between chaotic motion in the transverse direction and the axial dispersion of tracer was examined qualitatively. It was suggested that the dispersion of perfect tracer by the flow in a twisted pipe might provide a deterministic anologue of the shear dispersion mechanism described by Taylor (1953). In this section we illustrate the axial dispersion in the three regimes discussed in the introduction and examine the effects of small molecular diffusion.

Poincaré sections are computed by recording the intersections of particle trajectories with the pipe cross-section after every basic cell. This construction illustrates the segregation of the flow cross-section into regular and chaotic regions.

Four Poincaré sections for the non-integrable cases that have been used in this study are shown in figure 2. The parameters χ and Re are different in each of the four cases and the tracer is perfect. Note that there is a line of symmetry that is oriented at an angle $\chi/2$ with respect to vertical (JTA). Panels 2(*a–c*) illustrate the mixed regime. In each of these cases there is a single chaotic trajectory whose repeated intersections with the end of each cell fill in a two-dimensional subregion of the pipe cross-section. In addition to this non-integrable trajectory we show several trajectories in regular regions. These trajectories lie on streamsurfaces and their intersections with the end of the cell lie on one-dimensional curves.

Shown in figure 2 (*d*) is a single chaotic trajectory that wanders throughout the cross section of the pipe. This is an example of the irregular regime in which there are no streamsurfaces to restrict the orbit of a particle of ideal tracer. Of course, there are stable periodic points in this flow; however their volume is very small so their effect on tracer dispersion is probably negligible. This assumption will be justified *a posteriori*.

To give a qualitative indication of the effect of chaotic trajectories on the axial dispersion of perfect tracer 5000 particles are sequentially positioned along a diameter of the pipe that coincides with the axis of symmetry of the Poincaré section. The particle index is a unique label of the particle's initial position. These particles are advected for a fixed duration of time and each particle's final axial position, measured in radians, is plotted versus the particle index. A comparison of integrable and chaotic advection is shown in figure 3. Each panel of figure 3 shows the evolution of the axial distribution of particles at three different times.

The distribution in figure 3(*a*) for $\chi = 0$ is a smooth function of initial position, as expected for integrable advection. The two-humped profile arises because the initial line of tracer is stretched from the top of the pipe cross-section to the bottom, through the centres of the two counter-rotating vortices. The particles near the dividing streamline between these two vortices are rapidly swept into the slow-moving fluid near the wall of the pipe and they do not progress very far down the pipe.

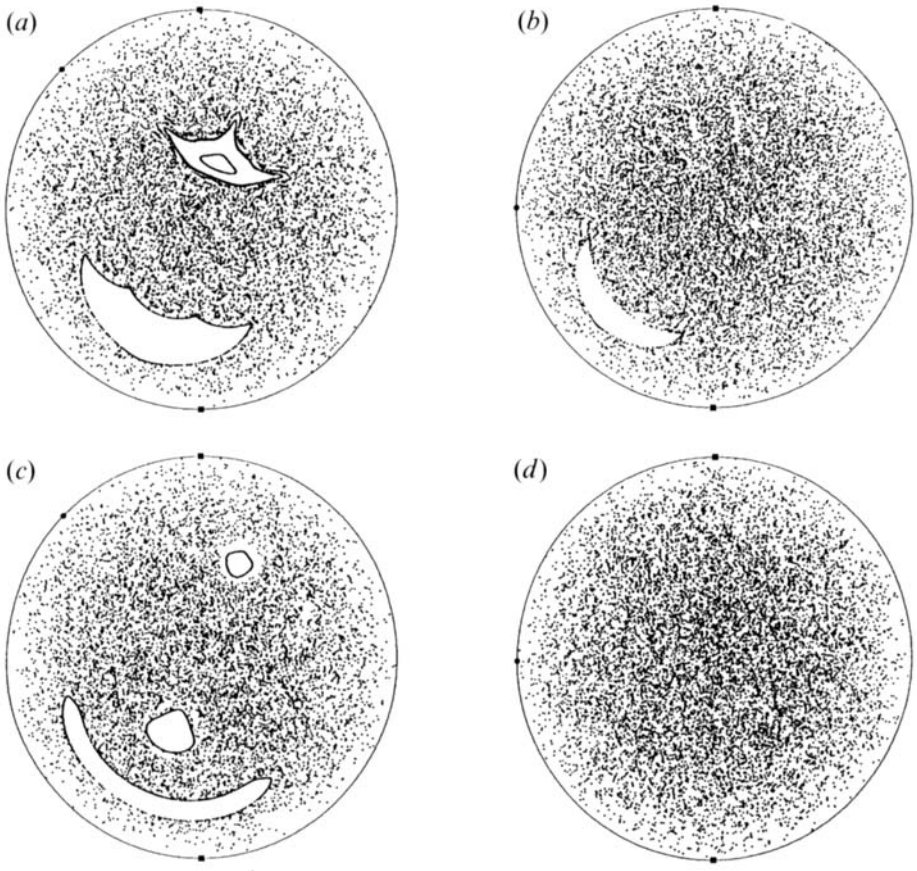

FIGURE 2. Poincaré sections of the flow through a twisted pipe for several values of the parameters. (*a*) $Re = 25$, $\chi = \pi/4$; (*b*) $Re = 25$, $\chi = \pi/2$; (*c*) $Re = 62.5$, $\chi = \pi/4$; (*d*) $Re = 62.5$, $\chi = \pi/2$.

The particles near the centres of the vortices never approach the wall and thus are transported much farther downstream.

Dispersion in the mixed regime is shown in figures 3(*b–c*). In contrast to the regular regime of figure 3(*a*) the distribution of particles in irregular regions is erratic and displays a sensitive dependence on the initial position. The smooth portions of these panels correspond to the islands of regular motion in the Poincaré sections of figures 2(*b*) and 2(*c*). Perfect tracer is trapped forever in these regular islands and the result is coherent motion along the axis of the pipe. For the mixed regime, with initial placement of perfect tracer particles uniformly throughout the section, this results in $\sigma^2(t) \sim \phi t^2$, where ϕ is the fraction of the pipe occupied by islands. If the tracer is not perfect then the initial placement is ultimately irrelevant because the tracer diffuses into and out of the islands.

Finally figure 3(*d*), which corresponds to the Poincaré section shown in figure 2(*d*), is an example of the distribution in the irregular regime. There are no smooth regions, and no coherent axial motion that can be resolved with a particle spacing of $4 \times 10^{-4}a$.

When molecular diffusion is introduced particles that start in regular regions can diffuse into irregular regions and vice versa. The top row of figure 4 shows the

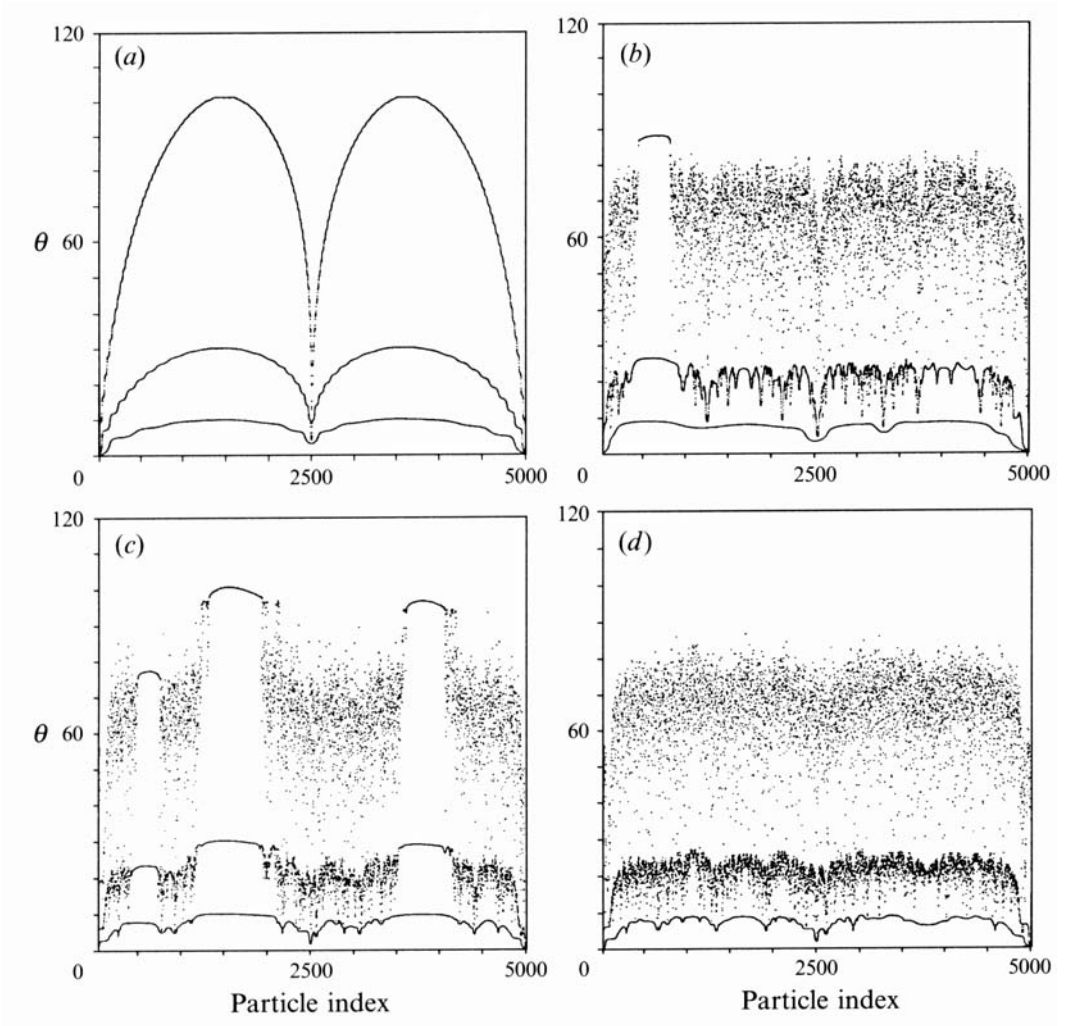

FIGURE 3. Axial dispersion of perfect particles. Abscissae are the particle indices. Ordinates are the axial position measured in radians. The three curves per panel are at times 6.25, 18.75, and 62.5. In the upper panels $Re = 25$ and (*a*) $\chi = 0$; (*b*) $\chi = \pi/2$. In the lower panels $Re = 62.5$ and (*c*) $\chi = \pi/4$; (*d*) $\chi = \pi/2$.

dispersion of diffusive tracer in the regular regime (figure 3*a*). It is clear that as the molecular diffusivity is increased the axial dispersion of particles is diminished. The bottom row of figure 4 shows the same trend in the mixed regime of figure 3(*b*).

When D is large the distributions of particles in the regular and mixed cases are quite similar because diffusive tracer is not confined to certain regions of the cross-section by streamsurfaces. However the approach to the Taylor limit is different in the two cases. In the regular regime (the top row) the initially smooth distribution becomes blurred by diffusion while in the mixed regime (the bottom row) the erratic distribution is focused into a relatively narrow band. Scaling arguments such as those of Koch & Brady (1985) suggest that the leading-order dependence of the effective

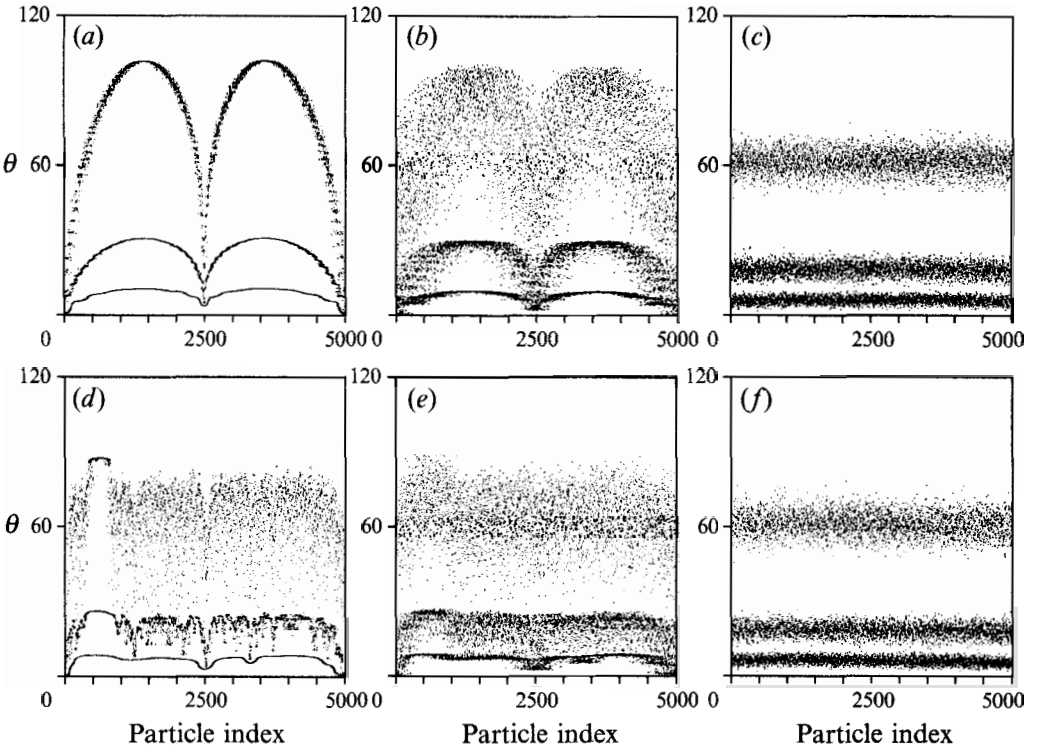

FIGURE 4. Axial dispersion of diffusive particles for the parameter values and times shown in figures 3(*a*) and (*b*). The top row shows the dispersion of diffusive tracer in the regular regime. The bottom row shows the dispersion of tracer in the mixed regime. Across each row D is 10^{-6}, 10^{-4} and 10^{-2}. (*a*)–(*c*) $\chi = 0$; (*d*)–(*f*) $\chi = \pi/2$.

diffusivity on the molecular diffusivity in this mixed case is

$$D_* \sim \frac{\phi U^2 a^2}{D_{\text{mol}}}, \tag{3.1}$$

where ϕ is the volume fraction of the regular motion. This is simply Taylor's result weighted by the fraction of the pipe occupied by regular trajectories.

3.2. *Diffusion coefficients*

The preceding subsection gave a qualitative indication of how chaotic trajectories affect the axial distribution of particles advected by a shear flow. In this subsection a quantitative measure of these effects is introduced. This is the function $D_*(t)$ defined by

$$D_*(t) = \frac{\sigma^2(t)}{2t}, \tag{3.2}$$

where $\sigma^2(t)$ is defined in (1.9). The limit of the function $D_*(t)$ as $t \to \infty$ is the diffusion coefficient, D_*.† Alternatively the diffusion coefficient may be determined from (1.3). The evolution of $D_*(t)$ for several parameter values is shown in figure 5.

† The function $D_*(t)$ will always include the argument. The absence of the argument indicates that the asymptotic value of this function is intended.

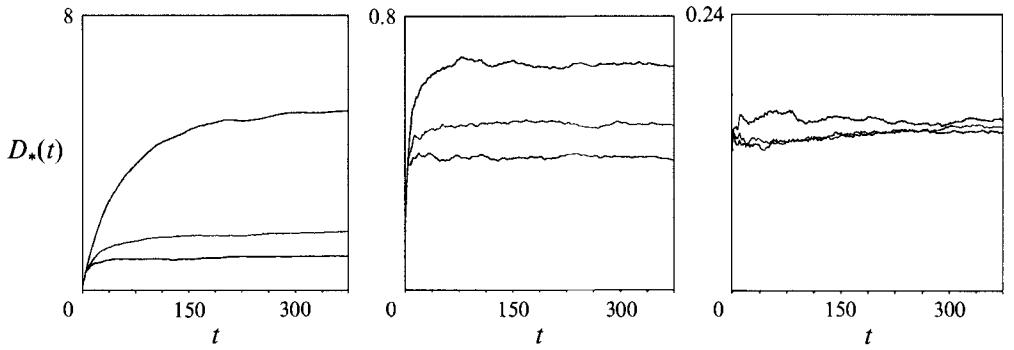

FIGURE 5. The convergence of the function $D_*(t)$ to its asymptotic value for $Re = 25$ and (*a*) $D = 10^{-4}$; (*b*) 10^{-3}; (*c*) 10^{-2}. In (*a*) and (*b*) the upper curve is for $\chi = 0$, the middle curve is for $\chi = \pi/4$ and the lower curve is for $\chi = \pi/2$. In (*c*) the upper curve is for $\chi = \pi/2$, the middle curve is for $\chi = \pi/4$ and the lower curve is for $\chi = 0$. Note the change of verticle scale between panels.

To construct this figure 2000 particles are positioned randomly in the pipe cross-section at $\theta = 0$ and then integrated (i.e. advected and diffused). To evaluate the relative contribution of chaotic trajectories to the shear dispersion observed in figure 4 the diffusion coefficient is measured for several values of χ and D. For $D = 10^{-4}$ (figure 5*a*) chaotic advection substantially reduces the dispersion coefficient relative to the integrable case, $\chi = 0$ (the upper curve). However, for $D = 10^{-2}$ the values of D_* are similar (figure 5*c*). These data are consolidated in figure 6 where D_* is plotted versus $\log D$.

3.3. *Dispersion of perfect tracer*

In this subsection we show that the dispersion of perfect tracer is fundamentally different from that of diffusive tracer. The evolution of $D_*(t)$ for perfect tracer is shown in figure 7. The lower curve is computed for $Re = 62.5$, $\chi = \pi/2$ and the upper curve for $Re = 62.5$, $\chi = \pi/4$. Clearly, neither curve has approached an asymptote by the end of the integration. Recall that the lower curve corresponds to the irregular Poincaré section (figures 2*d* and 3*d*) while the Poincaré section associated with the upper curve shows the growth of variance when particles are in both regular and chaotic regions (figure 2*c*).

To help understand the results of figure 7 we have constructed histograms of axial particle position at $t = 375$. Figure 8(*a*) shows the distribution of axial positions for the irregular flow. This distribution is skewed with a tail composed of particles lagging behind the centre of mass. Thus it is plausible that the failure of the lower curve in figure 7 to asymptote is due to particles that are trapped in a region of slow-moving fluid near the pipe wall. We examine this case analytically in §4 below.

In the mixed regime, when islands of regular motion are present (figure 8*b*), the no-slip trapping mechanism still operates and consequently there is still a tail of laggardly particles. But in addition a significant fraction of the particles lie well downstream of the centre of mass and the distribution is polymodal. It is plausible that tracer particles in regular islands move coherently relative to the centre of mass and this produces the downstream modes seen in the histogram in figure 8(*b*).

The correspondence between the downstream modes and the regular islands is verified by figure 9. In figure 9(*a*) we plot the initial positions of particles that make up the main mode of the distribution in figure 8(*b*) ($\theta - \bar{\theta} < 60$ rad). Figure 9(*b*)

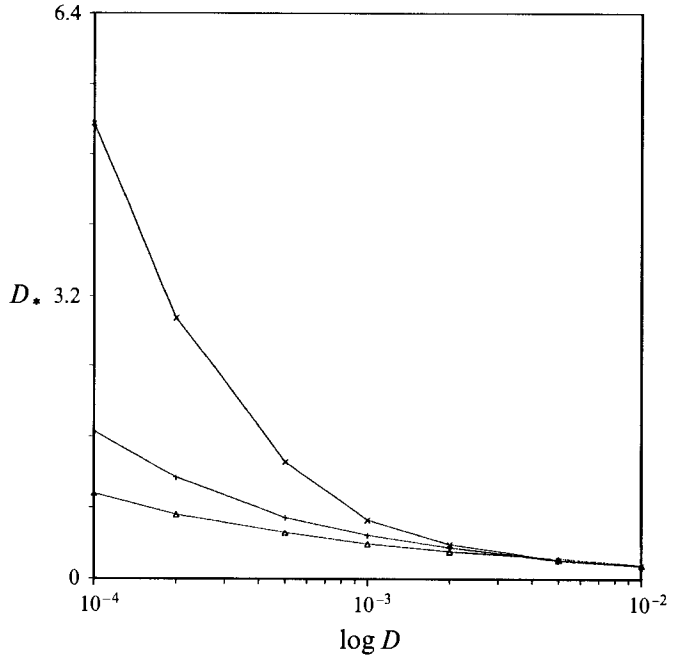

FIGURE 6. The measured value of D_* plotted versus $\log D$. $\times$, $Re = 25$, $\chi = 0$; $+$, $Re = 25$, $\chi = \pi/4$; $\triangle$, $Re = 25$, $\chi = \pi/2$.

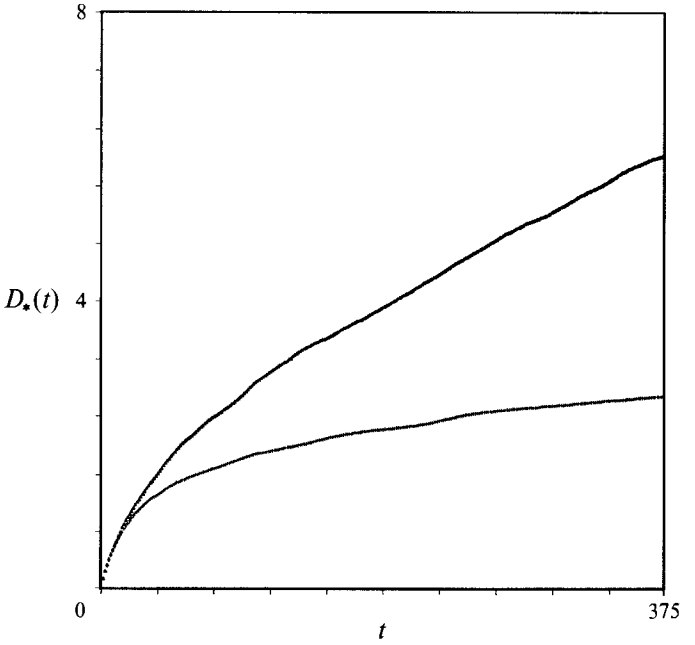

FIGURE 7. The evolution of $D_*(t)$ for perfect particles. The upper curve is for the mixed regime, $Re = 62.5$, $\chi = \pi/4$. The lower curve is for the irregular regime, $Re = 62.5$, $\chi = \pi/2$.

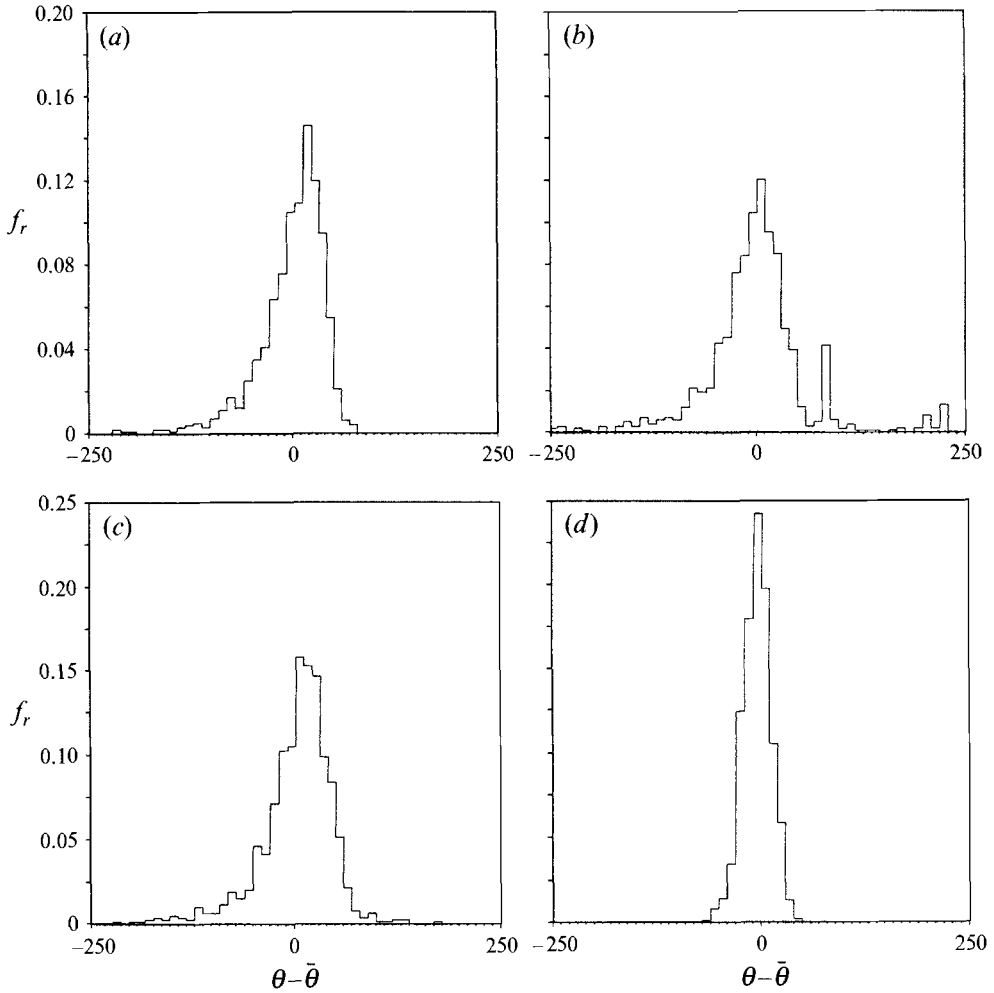

FIGURE 8. Histograms of axial position at $t = 375$. Ordinates are the fraction of particles, f_r, in each bin. Abscissae are longitudinal position relative to the centre of mass in bins of 10 rad. In panels (*a*)–(*c*) $Re = 62.5$ and (*a*) $\chi = \pi/2$, (*b*, *c*) $\chi = \pi/4$; (*d*) $D = 10^{-3}$, $Re = 62.5$, $\chi = \pi/2$. In (*b*) particles are positioned uniformly in the cross-section. In (*c*) particles are confined to the chaotic regions of the cross-section.

shows the initial positions of particles in the downstream mode $80 < \theta - \bar{\theta} < 90$ rad, while figure 9(*c*) shows the initial positions of particles that have been advected more than 160 rad. It is clear from a comparison of this figure with the Poincaré section in figure 2(*c*) that the regular islands transport particles in a coherent manner and produce the downstream modes.

Figure 8(*c*) shows the axial distribution produced when the initial position of particles is restricted to the chaotic sea. Because no particles are initially in the islands the downstream peaks have disappeared. The absence of these peaks in figure 8(*a*), where the initial distribution of the particles was uniform, supports our earlier contention that there are no regular islands in this simulation.

Finally, for comparison, figure 8(*d*) shows a distribution for diffusive particles in the irregular regime. This distribution looks more Gaussian than those obtained

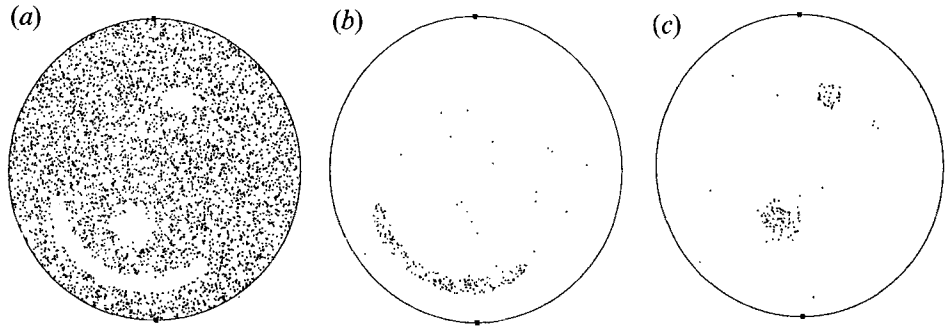

FIGURE 9. The initial positions of particles whose longitudinal position relative to the centre of mass in figure 8(*b*) is (*a*) $\theta - \overline{\theta} < 60$ rad, (*b*) $80 < \theta - \overline{\theta} < 90$ rad, (*c*) $\theta - \overline{\theta} > 160$ rad.

using perfect tracer. The distribution is more symmetric, and there is only one mode. Moreover the tracer is concentrated in a smaller range of axial position (note the change of vertical scale).

The skewness of the distributions shown in figure 8 has been computed using the definition

$$S_k \equiv \frac{1}{N} \sum_{i=1}^{N} \left(\frac{\theta_i - \overline{\theta}}{\sigma} \right)^3. \tag{3.3}$$

In Taylor's theory the axial distribution of tracer becomes Gaussian at large times so all of the odd moments asymptote to zero. We first note that the skewness of the axial distribution of perfect tracer in figure 8(*a*) is non-zero and has the value $S_k = -2.1$. In figure 8(*b*) the distribution is more symmetric, $S_k = -0.2$, because the tracer in islands 'balances' that in the boundary region. Figure 8(*c*) has the intermediate value -1.4 and figure 8(*d*), for diffusive tracer, is the most symmetric with a skewness of -0.1.

In figure 10 the time evolution of the measured value of $|S_k|$ is compared for perfect and diffusive particles. Aris (1956) predicts that as $t \to \infty$ the skewness of diffusive tracer decays like $t^{-1/2}$. Indeed, the lower curve in figure 10 does decay slowly but we have not attempted a quantitative test of the $t^{-1/2}$ scaling. The growing skewness of perfect tracer in figure 10 differs qualitatively from the slowly decaying skewness of the diffusive tracer. The temporal evolution of the skewness is the subject of §4.2 and the Appendix by J. F. Brady.

4. Dispersion in the irregular regime

In this section we study the effect of the no-slip condition on dispersion in the irregular regime. Our numerical results have suggested that this boundary condition might be responsible for the non-convergence of the effective diffusivity evident in the lower curve on figure 7. Thus the trailing tail of laggardly particles in figure 8(*a*) is likely to be responsible for both the anomalous diffusion in figure 7 and the growing skewness in figure 10. We show below that the Lagrangian velocity autocorrelation function for perfect tracer decays slowly as in (1.5) and we calculate p. This explains the anomalous diffusion: the function $D_*(t) \equiv \sigma^2(t)/2t$ in the lower curve on figure 7 is increasing as $\ln t$.

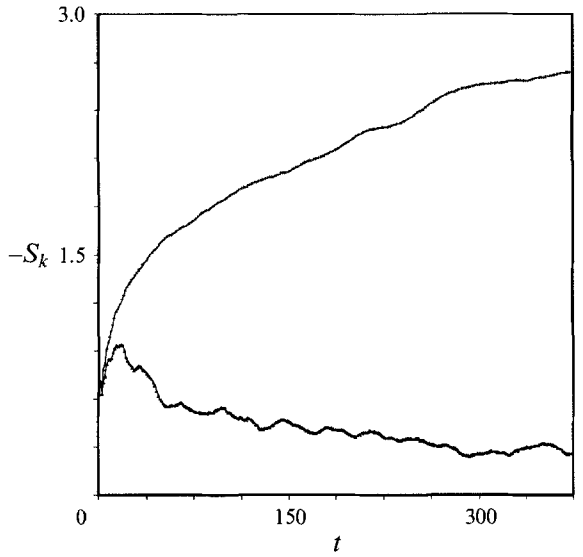

FIGURE 10. The opposite value of the normalized skewness, $-S_k$ plotted versus time. The upper curve is for perfect particles advected in the irregular regime, $Re = 62.5$, $\chi = \pi/2$. The lower curve is for the same flow parameters, but for diffusive particles with $D = 10^{-3}$.

4.1. *Time evolution of the variance*

We use a Lagrangian approach to calculate the constant p in (1.5). Taylor's formula, (1.3), then shows that the effective diffusivity for ideal tracer particles diverges like $\sigma^2(t) \sim 2pt \ln t$. For diffusive tracer this divergence is removed and scale analysis shows that the effective diffusivity is given by (1.8).

The velocity correlation function is an ensemble average of lagged Lagrangian velocities:

$$\mathscr{C}(t) \equiv \frac{1}{N} \sum_{i=1}^{N} w_i'(0) w_i'(t). \tag{4.1}$$

In the irregular regime we assume that as $t \to \infty$ the only non-zero terms in the sum (4.1) are due to particles that remain in a thin region near the pipe wall for the entire interval. In the mixed regime there are additional sources of long-time correlations, such as trapping near regular islands, which greatly complicate the calculation of the correlation function (e.g. Karney 1983; Meiss & Ott 1986). Here we restrict attention to the irregular regime and suppose that the only significant long-time correlations come from particles trapped in the slowly moving fluid near the wall of the pipe. This assumption is tested by a successful comparison of our analytic calculation with numerical simulation.

We suppose that a large number of molecules of perfect tracer are uniformly distributed across the pipe at $t = 0$ and we focus attention on those in a thin annular strip, $1 - \epsilon < r < 1$, near the wall of the pipe. At large times we approximate (4.1) by

$$\mathscr{C}(t) \approx \left(\frac{1}{N}\right)(2\epsilon N)\left(\frac{A(t)}{2\pi\epsilon}\right)(-1)^2 = \frac{A(t)}{\pi}. \tag{4.2}$$

Here $A(t)$ is the transverse area of the fluid initially in the strip that is still in the strip at t. The first factor in (4.2) is division by the total number of particles in

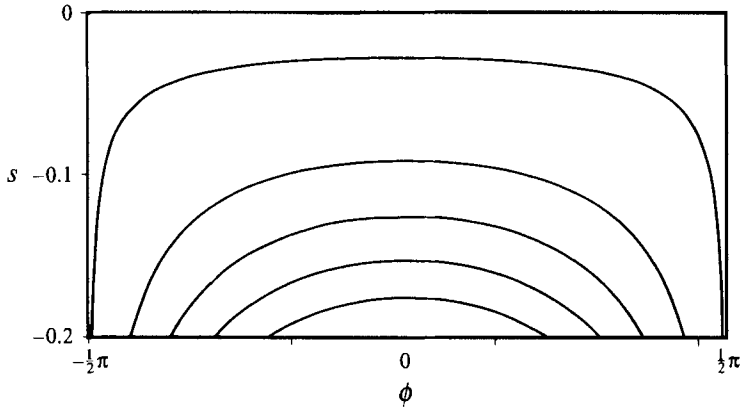

FIGURE 11. Streamlines of the local streamfunction given by (4.5). Only half of the strip is shown here.

the ensemble: this is the $1/N$ immmediately on the right-hand side of (4.1). The second factor is the number of particles in the strip at $t = 0$. The third factor is the fraction of particles initially in the strip which are still in the strip at t. The product of the second and third terms is the number of non-zero terms in the sum (4.1) at time t. The final factor is the value of each of these non-zero terms and in the strip $w'(0) \approx w'(t) \approx -1$ so this value is unity. The goal of the subsequent analysis is to determine the unknown function $A(t)$ and this is done with a local analysis of (2.4) and (2.5).

In the boundary strip we simplify the advection equations (2.1) by introducing the local coordinates

$$s \equiv r - 1, \qquad \phi \equiv \arctan(x/y) \tag{4.3}$$

and using $|s| \ll 1$. The result is

$$\dot{s} = -\psi_\phi = \frac{Re}{6} s^2 \sin\phi, \quad \dot{\phi} = \psi_s = \frac{Re}{3} s \cos\phi, \quad \dot{\theta} = -4s \tag{4.4}$$

where

$$\psi(s, \phi) \equiv \frac{Re}{6} s^2 \cos\phi. \tag{4.5}$$

Because the motion is steady particles remain on their original streamlines, i.e. $\dot{\psi} = 0$. This local approximation of the streamfunction is sketched in figure 11.

It is easy to calculate the time taken to completely traverse a streamline starting at $(s, \phi) = (-\infty, \pi/2)$ and finishing at $(s, \phi) = (-\infty, -\pi/2)$. One finds

$$T(\psi) = \frac{\mu}{|\psi|^{1/2}}, \tag{4.6}$$

where

$$\mu \equiv \left(\frac{6}{Re}\right)^{1/2} \int_0^{\pi/2} \frac{d\phi}{(\cos\phi)^{1/2}} \approx 6.42 Re^{-1/2}. \tag{4.7}$$

We can invert (4.6) and express the streamfunction in terms of this traversal time

$$\psi = \frac{\mu^2}{T^2}. \tag{4.8}$$

Now imagine that the fluid in the strip at $t = 0$ is dyed red so that $A(t)$ is the area of red fluid still in the strip at t. As $t \to \infty$ the red fluid leaves the strip through a shrinking window centred on $\phi = -\pi/2$ and defined by the intersection of the streamline in (4.8) with the open boundary of the strip, $s = -\epsilon$. The flux of red fluid out of the strip, $J(t)$, is just the value of the streamfunction that instantaneously defines the window:

$$J(t) = 2\psi(t) = \frac{2\mu^2}{t^2}. \tag{4.9}$$

The factor of 2 in the above expression arises from the symmetry of the streamfunction about $\phi = -\pi/2$. The area of red fluid that remains in the strip at time t is related to this flux by

$$J(t) = -\frac{\mathrm{d}A(t)}{\mathrm{d}t}. \tag{4.10}$$

so that at large times $A(t) = 2\mu^2/t$.

The probability that a particle remains in the strip for an interval of length t is the ratio

$$\frac{A(t)}{2\pi\epsilon} = \frac{\mu^2}{\pi\epsilon t} \approx \frac{13.13}{\epsilon t Re}. \tag{4.11}$$

This estimate has neglected the effects of the twists and it is of interest to compare it with a complete calculation. This is done in figure 12 where we show the fraction of particles that remain in a strip of width $\epsilon = 0.05$ if $Re = 62.5$ and $\chi = \pi/2$. With these values of Re and ϵ the right-hand side of (4.11) is $4.20/t$ and there is good asymptotic agreement between this law and the numerical results.

Using (4.11) we now return to (4.2) and obtain for the non-dimensional correlation function

$$\mathscr{C}(t) \approx \frac{26.26}{Re\, t} \quad \text{as } t \to \infty. \tag{4.12}$$

(In dimensional variables this implies that the constant p in (1.5) is $p = 26.26\nu R/a$.) In the numerical simulation in figure 7, $Re = 62.5$ so $\mathscr{C}(t) \approx 0.42/t$ and from (1.3) we have a prediction for the anomalous growth of variance in the twisted pipe:

$$\sigma^2(t) \approx 0.84 t \ln t \tag{4.13}$$

or in terms of the diffusivity introduced in (3.1)

$$D_*(t) \approx 0.42 \ln t. \tag{4.14}$$

This result is compared with the simulation in figure 13.

The introduction of small molecular diffusivity truncates the tail of the correlation function and results in a finite diffusivity as $t \to \infty$. In fact our expression in (4.2) for the correlation function is correct even if the tracer is diffusive. However the preceding calculation of $A(t)$ is invalid at large times because molecular diffusion accelerates the escape of the red fluid from the strip so that at large times $A(t)$ decays exponentially. A detailed calculation of $A(t)$ requires the solution of the local approximation to the tracer conservation equation (2.10)

$$C_t + \frac{Re}{6} s^2 \sin\phi C_s + \frac{Re}{3} s \cos\phi C_\phi = D C_{ss} \tag{4.15}$$

with an initial condition $C(s, \phi, 0) = 1$ and an absorbing boundary condition $C(\epsilon, \phi, t) = 0$. Thus at $t = 0$ there is a uniform concentration of red fluid in

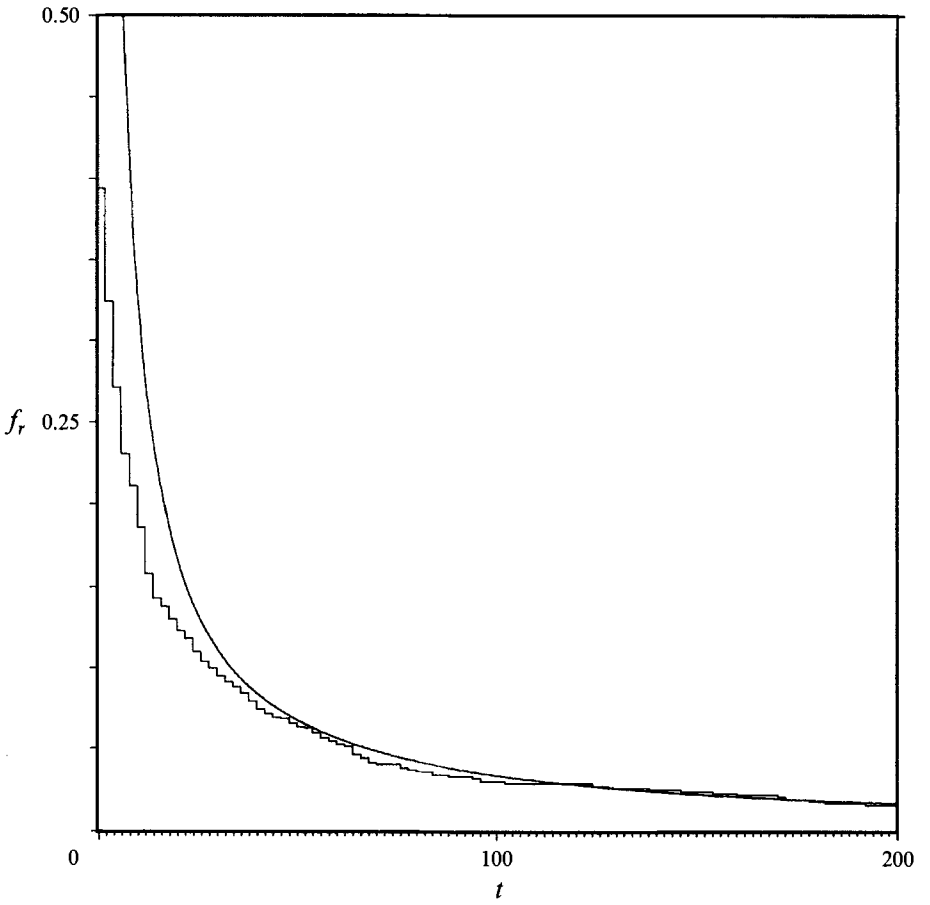

FIGURE 12. A comparison of the analytical result given by (4.11) with a 5000 particle simulation for $Re = 62.5$, $\chi = \pi/2$. 107 particles remain in the strip at $t = 200$.

the strip and when molecules reach the boundary they are removed from the ensemble. Then the amount of red fluid that has not been evacuated from the strip at t is

$$A(t) = \int C(s, \phi, t) \mathrm{d}A, \tag{4.16}$$

where the integral is over the whole strip.

Our earlier calculation of $A(t)$ took $D = 0$, evaluated the flux $J(t)$ of red fluid out of the strip at $s = \epsilon$, and then inferred $A(t)$ from (4.10). With molecular diffusivity this approach fails because at large times molecules near the wall diffuse into regions which have been mechanically evacuated at earlier times. Considerable progress towards a solution of (4.15) can be made using the transformations given by Acrivos & Goddard (1965), but the calculation is intricate and here we only employ the scaling arguments from this reference to obtain a leading-order approximation to the diffusivity. We rescale s and t in (4.15) so that there are no non-dimensional parameters in the tracer conservation equation. The new variables are

$$\hat{s} = Pe^{-1/3}s, \qquad \hat{t} = RePe^{1/3}t, \tag{4.17}$$

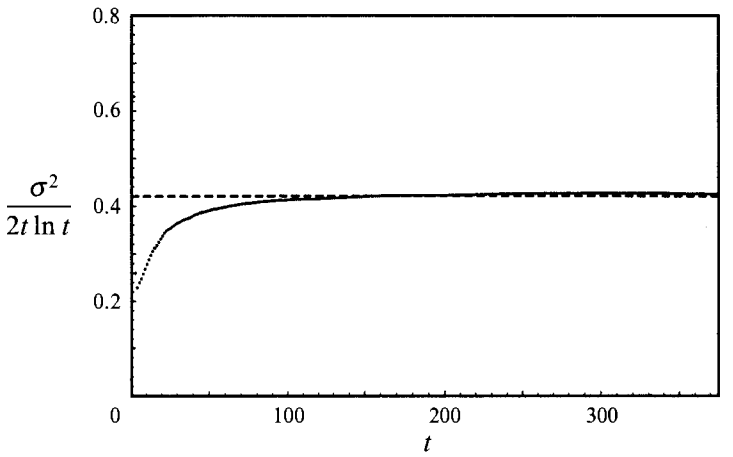

FIGURE 13. A comparison of the analytical result for the variance at long times, given by (4.13) (dashed line), with a twisted-pipe simulation for $Re = 62.5$, $\chi = \pi/2$. The numerical result was produced by averaging 10 runs, each consisting of ensembles of 10^5 particles.

where Pe is defined in (2.12). Provided $\epsilon Pe^{-1/3} \gg 1$ and $\hat{t} \ll 1$ our earlier calculation of $A(t)$ is valid. However when $\hat{t} \sim 1$ diffusion becomes important and assists in the evacuation of the strip so that $A(t)$ and $\mathscr{C}(t)$ decay exponentially. This rapid decay makes the integral in Taylor's expression for the diffusivity, (1.3), converge and the leading-order approximation is obtained by stopping the integration when $\hat{t} \sim 1$. This gives $D_* \sim (p/3)\ln Pe \sim -(p/3)\ln D$ as $D \to 0$. Figure 14 shows a comparison of this result, $D_* = -0.14\ln D = -0.32\log_{10} D$, with numerical simulations in which $Re = 62.5$ and $p \approx 0.42$. The filled circles are the data points determined from the numerical simulation. The dashed line has slope $-p/3 = -0.32$ and the solid line is the least-squares fit to the data points which has slope -0.34. (The unknown intercept of the dashed line is chosen so that the intersection with the least-squares fit occurs at $D = 10^{-6}$.) We have performed numerical experiments for different values of Re and consistently find good agreement between theory and numerical simulation.

4.2. *Time evolution of the skewness*

One can use our derivation of $D_*(t)$ and the transport theory developed by Koch & Brady (1987) to predict the time evolution of the skewness. Details are provided in the Appendix written by J. F. Brady. To simplify the analysis we use the unnormalized skewness

$$S(t) = \frac{1}{N}\sum_{i=1}^{N}(\theta_i - \bar{\theta})^3. \tag{4.18}$$

The Koch & Brady transport theory (1987) gives the leading-order expression

$$S(t) = -3pt^2. \tag{4.19}$$

A comparison of this calculation with our simulations is shown in figure 15. Although the transport theory correctly predicts the t^2 growth of the skewness the measured constant of proportionality is closer to 1.4 than $3p = 1.26$. This discrepancy may be an effect of undersampling the tail of the concentration distribution.

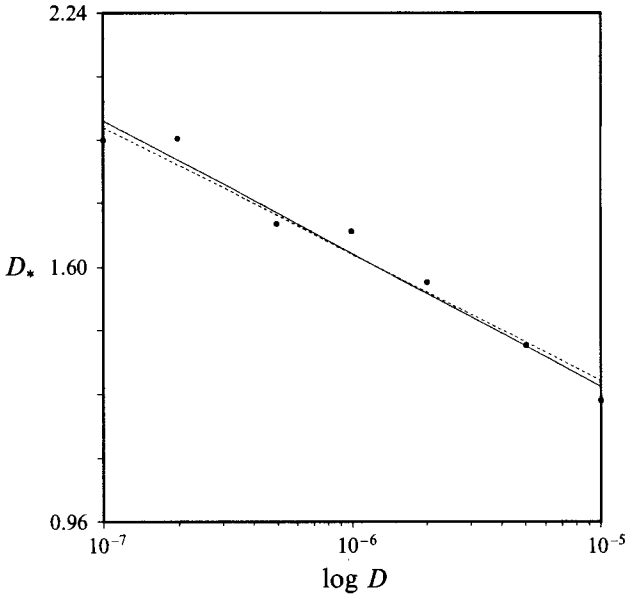

FIGURE 14. The large-Péclet-number behaviour of D_* as a function of $\log D$ for $Re = 62.5$, $\chi = \pi/2$. The filled circles are the values determined by numerical experiments, the solid line is a least-squares fit to these points and the dashed line is the analytical result $D_* = -0.32 \log D + c$ where the undetermined constant c is chosen so that the two curves intersect at $D = 10^{-6}$. The slope of the solid line is -0.34.

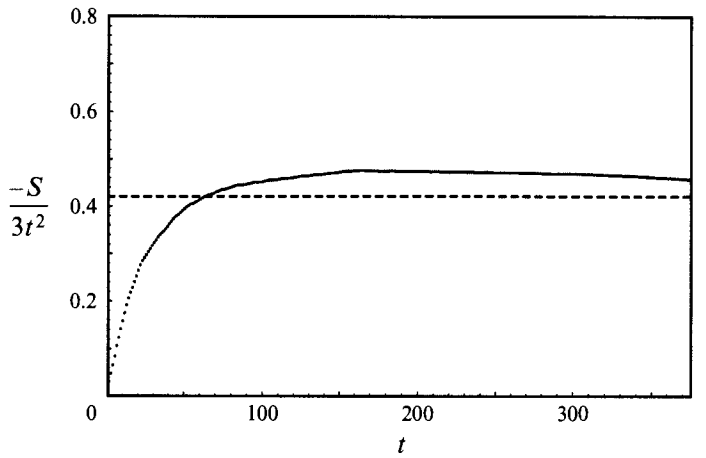

FIGURE 15. A comparison of the analytical result for the unnormalized skewness at long times, given by (4.19) (dashed line), with a twisted-pipe simulation for $Re = 62.5$, $\chi = \pi/2$.

5. Discussion and conclusion

From our results it is clear that the no-slip condition is crucially important in the twisted-pipe dispersion problem. In the irregular regime the no-slip condition results in a 'non-mechanical' effective diffusivity, i.e. D_* does not become independent of molecular diffusivity as $Pe \to \infty$, and for perfect tracer the mean-square displacement

about the centre of mass grows as $t \ln t$. These points have been made in the context of dispersion in porous media (e.g. Saffman 1959; Koch & Brady 1985) and we reiterate their importance in the problem of dispersion by chaotic advection.

In the irregular regime we have been able to analytically calculate the constant of proportionality for the growth rate of the position variance. However, in the mixed regime the dispersion of tracer is more complicated and our results are restricted to numerical simulations and scale analysis. Because the flow domain consists of regions of regular motion and chaotic motion the long-time dispersion of perfect tracer is a function of initial position. If perfect tracer is released in both the islands and the sea then the coherent motion in the islands dominates and $\sigma^2(t) \sim \phi t^2$, where ϕ is the volume fraction of the islands. If perfect tracer is initially restricted to the chaotic sea then the asymptotic growth of the variance is difficult to predict: in addition to the no-slip condition, long-time correlations are produced by trapping near islands (Karney 1983; Meiss & Ott 1986). This trapping results in diffusion which is more anomalous than $t \ln t$, such as $\sigma^2(t) \sim t^\alpha$, where $1 < \alpha < 2$. The tail of the correlation function, $t^{\alpha-2}$, depends on the details of the flow structure near the islands, rather than the wall of the pipe. In fact this is a frontier issue in dynamical systems theory. Thus the dispersion of perfect tracer in the mixed regime of chaotic advection can differ from that in a porous medium, a point also made by Koch *et al.* (1989).

In summary, the effect of chaotic advection on the axial dispersion of diffusive tracer is to reduce the value of the dispersion coefficient. This reduction is a consequence of chaotic trajectories permitting particles to more rapidly sample the axial velocity profile. The dispersion of perfect tracer by chaotic advection is also slower than that of integrable advection. In the irregular regime the variance of axial position grows like $t \ln t$ with a coefficent which can be calculated exactly using the reasoning in §4. The measured skewness also grows with time, like t^2 (figure 15). Again we can use the Lagrangian analysis in §4, in concert with the macrotransport theory of Koch & Brady (1987) to find the coefficient that precedes the t^2 scaling.

We would like to thank H. Aref, J. F. Brady and D. L. Koch for many beneficial discussions and suggestions.

The support of IGPP/LANL 88-16-215 and NSF grant MSM 84-51107 and resources made available at the San Diego Supercomputer Center are gratefully acknowledged. WRY was supported by the National Science Foundation and the Office of Naval Research.

Appendix. Skewness of the anomalous $t \ln t$ diffusion

By J. F. Brady
Division of Chemistry and Chemical Engineering, California Institute of Technology, Pasadena, CA 91125, USA

Here we show that the non-local theory of Koch & Brady (1987) can be used to predict the skewness of the dispersion profile in the anomalous diffusion regime caused by the no-slip boundary condition at the walls of the tube.

The dispersion of a passive tracer, denoted by the concentration c, flowing in a tube can be expressed in terms of the moments of the concentration distribution

$$\langle (z-t)^n \rangle = \int_{-\infty}^{\infty} (z-t)^n \langle c(z,t) \rangle \mathrm{d}z \tag{A 1}$$

$$= \lim_{k\to 0} \frac{1}{2\pi} \int_{-\infty}^{\infty} \left(\mathrm{i}\frac{\mathrm{d}}{\mathrm{d}k} - t \right)^n \langle \hat{c}(k,\omega) \rangle \mathrm{e}^{\mathrm{i}\omega t} \mathrm{d}\omega. \tag{A 2}$$

Here, the flow direction is denoted by z and without loss of generality the mean velocity of the tracer in the flow direction has been set equal to unity. The second equation follows from application of the convolution theorem, with the $\hat{}$ denoting the transform in both space and time. The angle brackets denote an average over the realizations of the velocity field and the initial distribution of tracer, which we take here to be uniform across the cross-section of the tube.

Koch & Brady (1987) developed a general, spatially and temporally, non-local theory for dispersion processes applicable to diffusive and non-diffusive tracers in any flow. Applying this theory to the anomalous diffusion caused by the no-slip boundary condition at the walls of the tube for a perfect, non-diffusive, tracer leads to the following expression for the transform of the average concentration field (cf. §4 of Koch & Brady 1987):

$$\langle \hat{c}(k,\omega) \rangle = \frac{1 + \mathrm{i}k\hat{D}}{\mathrm{i}\omega + \mathrm{i}k - \omega k \hat{D}}, \tag{A 3}$$

where the 'diffusivity', $\hat{D}$, in the anomalous regime is given by

$$\hat{D} = -2p \ln |\mathrm{i}\omega|, \tag{A 4}$$

and p is defined in the text in equation (1.5) and in (A 6) below.

By straightforward work using (A 3) and (A 4) the first three moments are

$$\langle (z-t) \rangle = 0, \tag{A 5}$$

$$\langle (z-t)^2 \rangle = 2pt \ln t + O(t), \tag{A 6}$$

$$\langle (z-t)^3 \rangle = -3pt^2 + O(t \ln^2 t). \tag{A 7}$$

The third moment is the skewness reported in (4.19).

REFERENCES

Acrivos, A. & Goddard, J. D. 1965 Asymptotic expansions for laminar forced-convection heat and mass transfer. Part 1. Low speed flows. *J. Fluid Mech.* **23**, 273–291.

Aref, H. 1984 Stirring by chaotic advection. *J. Fluid Mech.* **143**, 1–21.

Aris, R. 1956 On the dispersion of solute in a fluid flowing through a tube. *Proc. R. Soc. Lond.* A **235**, 66–77.

Baudet, C., Guyon, E. & Pomeau, Y. 1985 Dispersion dans un écoulement de Stokes. *J. Physique Lett.* **46** L991–L998 (in french).

Dean, W. R. 1927 Note on the motion of fluid in a curved pipe. *Phil. Mag.* **4**, 208–223.

Dean, W. R. 1928 The streamline motion of fluid in a curved pipe. *Phil. Mag.* **5**, 673–693.

Erdogan, M. C. & Chatwin, P. C. 1967 The effects of curvature and buoyancy on the laminar dispersion of solute in a horizontal tube. *J. Fluid Mech.* **29**, 465–484.

Guyon, E., Nadal, J.-P. & Pomeau, Y. (eds.) 1988 *Disorder and Mixing.* Kluwer.

Johnson, M. & Kamm, R. D. 1986 Numerical studies of steady flow dispersion at low Dean number in a gently curving tube. *J. Fluid Mech.* **172**, 329–345.

Jones, S. W., Thomas, O. M. & Aref H. 1989 Chaotic advection by laminar flow in a twisted pipe. *J. Fluid Mech.* **209**, 335–357 (referred to herein as JTA).

Josselin de Jong, G. de 1958 Longitudinal and transverse diffusion in granular deposits. *Trans. Am. Geophys. Union* **39**, 67–74.

Karney, C. F. F. 1983 Long-time correlations in the stochastic regime. *Physica* D **8**, 360–380.

Koch, D. L. & Brady, J. F. 1985 Dispersion in fixed beds. *J. Fluid Mech.* **154**, 399–427.

Koch, D. L. & Brady, J. F. 1987 Nonlocal dispersion in porous media: nonmechanical effects. *Chem. Engng Sci.* **42**, 1377–1392.

KOCH, D. L., COX, R. G., BRENNER, H. & BRADY, J. F. 1989 The effect of order on dispersion in porous media. *J. Fluid Mech.* **200**, 173–188.

LICHTENBERG, A. J. & LIEBERMAN, M. A. 1982 *Regular and Stochastic Motion.* Springer.

MEISS, J. D. & OTT, E. 1986 Markov tree model of transport in area-preserving maps. *Physica* D **20**, 387–402.

NUNGE, R. J., LIN, T.-S. & GILL, W. N. 1972 Laminar dispersion in curved tubes and channels. *J. Fluid Mech.* **51**, 363–383.

SAFFMAN, P. G. 1959 A theory of dispersion in a porous medium. *J. Fluid Mech.* **6**, 321–349.

SAXENA, A. K. & NIGAM, K. D. P. 1984 Coiled configuration for flow inversion and its effect on residence time distribution. *AIChE J.* **30**, 363–368.

TAYLOR, G. I. 1921 Diffusion by continuous movements. *Proc. Lond. Math. Soc.* **20**, 196–212.

TAYLOR, G. I. 1953 Dispersion of soluble matter in solvent flowing slowly through a tube. *Proc. R. Soc. Lond.* A **219**, 186–203.

TAYLOR, G. I. 1954 The dispersion of matter in turbulent flow through a pipe. *Proc. R. Soc. Lond.* A **223**, 446–468.

YOUNG, W. R. & JONES, S. W. 1991 Dispersion in an unconsolidated porous medium. *Phys. Fluids* A **3**, 2468–2470.